# Coupling effect between film boiling heat transfer and evaporation drag around a hot-particle in cold liquid

LI Xiao-Yan, YANG Yan-Hua, XU Ji-Jun

*(Department of Nuclear Science and System Engineering, School of Mechanics and Power Engineering, Shanghai Jiaotong University, Shanghai 200030)*

**Abstract** Extremely rapid evaporation could occur when high-temperature particles contact with low-temperature liquid. This kind of phenomenon is associated with the engineering safety and the problems in high-transient multi-phase fluid and heat transfer. The aim of our study was to design and build an observable experiment facility. The first series of experiments were performed by pouring one or six high-temperature particles into a low saturated temperature liquid pool. The particle's falling-down speed was recorded by a high-speed camera, thus we can find the special resistant feature of the moving high-temperature particles, which is induced by the high-speed evaporation surrounding the particles. The study has experimentally verified the theory of evaporation drag model.

**Keywords** Vapor explosion, FCI (Fuel-coolant interactions), Evaporation drag model

**CLC number** TK12

## 1 Introduction

Extremely high-rate evaporation could occur while high-temperature particles contact with low-temperature liquid, which may induce vapor explosion. Since this kind of phenomenon is associated with the safety of engineering in certain industrial and material area involving high-transient multi-phase fluid and heat transfer process, a number of experiments and theoretical studies have been performed all around the world,[1] such as the QUEOS, MAGICO, and BILLEAU-2200 experiments. However, after severe accident of TMI-2, the expert elicitation of FCI (fuel-coolant interactions) suggested the requirement to learn more about the fundamental mechanisms of FCI to be able to determine the conditions under which FCI is important to severe accident risk and accident management.[2]

The fundamental aspect of FCI is the evolution of liquid interfacial (fuel-coolant) area and associated heat transfer during the contact, particularly, the basic mechanisms study during premixing stage of FCI. When two liquids first come into contact, the coolant begins to vaporize at the fuel-coolant liquid interface as a vapor film separates the particles from liquid interface. During this stage the system remains for a delay period ranging from a few milliseconds up to a few seconds because of density and velocity differences as well as vapor production.[3] But the basic study, such as a single high-temperature particle pouring into the cold liquid pool, has few been made. If we observe the motion of the melt inside of the vapor film, we would have a question why the melt drop can be maintained without contacting with the interface of the film and the coolant at the bottom of the drop even though it has a gravity much larger than the surrounding fluid. One explanation is that the thickness-growing rate of the film at the bottom of the drop is faster than the falling velocity of the drop. Another explanation is that there is large force inside the vapor film, which resists the descent of melt drop. By the first explanation, the drag on the melt cannot be large enough to raise up the sphere as the buoyancy from the vapor is very small, so that the melt can be driven only by its gravity. The second explanation is opposite and driven from the evaporation drag model.[4] As stated in next section, from the view of evaporation it is considered that if a hot particle is surrounded by a

Supported by National Natural Science Fund (No.50046026)
Received date: 2002-08-13

vapor film with different thickness circumferentially, the local evaporation rate and the local density of the vapor may have a non-spherical-symmetric distribution, which could induce a non-spherical-symmetric profile for pressure and form a flow around the particle. This non-symmetric profile would bring about a resultant force on the hot particle so as to resist its motion. The paper describes the experiment that may verify the evaporation drag model theory.

## 2 Evaporation drag model

The drag force on a particle moving inside liquid is the resultant of the pressure and the viscous stress acting on its surface. Hence the total surface force acting on the particle will be the surface integral of the pressure and the viscous stress. In a locally fitted spherical polar surface coordinate system, the drag force can be written as[4]

$$\vec{F}_{\mathrm{h}} = -r_{\mathrm{h}}^{2}\int_{0}^{2\pi}\int_{0}^{\pi}(p\sin\theta - \tau\cos\theta)\vec{n}\,\mathrm{d}\theta\,\mathrm{d}\varphi \tag{1}$$

where $p$ and $\tau$ are pressure and viscous stress acting on the surface of the hot particle respectively, $\vec{n}$ is unit vector of surface, $r_{\mathrm{h}}$ is radius of the hot particle. The drag changes during the whole process of the particle passing through the free surface. However, since the process is extremely short, it may be more interesting to consider the velocity drop of the particle passing through the surface than the drag during the process. According to the evaporation drag model, the final velocity of the hot sphere at the end of the penetration is

$$v_{\mathrm{h}}^{\mathrm{tp}} = \sqrt{v_{\mathrm{h}}^{02} + 4r_{\mathrm{h}}g - \frac{10}{9}\frac{p_{\mathrm{g}}}{\rho_{\mathrm{h}}}\left(\frac{\phi}{v_{\mathrm{a}}} - 1\right) - \frac{3}{5}gt_{\mathrm{p}}v_{\mathrm{a}}\frac{\rho_{\mathrm{l}}}{\rho_{\mathrm{h}}}} \tag{2}$$

where $v_{\mathrm{h}}^{0}$ is velocity when the sphere touches the water surface ($\mathrm{m\cdot s^{-1}}$); $g$ is the gravitational acceleration ($\mathrm{m\cdot s^{-2}}$); $p_{\mathrm{g}}$ is gas pressure on the upper part of the sphere (Pa); $\rho_{\mathrm{h}}$ is density of the hot sphere ($\mathrm{kg\cdot m^{-3}}$); $\rho_{\mathrm{l}}$ is density of the coolant ($\mathrm{kg\cdot m^{-3}}$); $\phi$ is the vapor generation speed ($\mathrm{m\cdot s^{-1}}$); $t_{\mathrm{p}}$ is the total time required for the particle entirely penetrating into the coolant (s); $v_{\mathrm{a}}$ is the steady film growth ($\mathrm{m\cdot s^{-1}}$).

The parameters $v_{\mathrm{h}}^{0}$, $r_{\mathrm{h}}$, $p_{\mathrm{g}}$, $\rho_{\mathrm{h}}$, $\rho_{\mathrm{l}}$ and $t_{\mathrm{p}}$ can be measured in the experiment, while

$$\phi = \frac{\Gamma_{\mathrm{h}}}{\rho_{\mathrm{gv}}}, \quad \Gamma_{\mathrm{h}} = \frac{q_{\mathrm{h}}}{h_{\mathrm{fg}}}, \quad q_{\mathrm{h}} = \varepsilon_{\mathrm{l}}\varepsilon_{\mathrm{h}}\sigma\left(T_{\mathrm{h}}^{4} - T_{\mathrm{l}}^{4}\right) \tag{3}$$

where $\varepsilon_{\mathrm{l}}$ is the absorbance coefficient of the liquid; $\varepsilon_{\mathrm{h}}$ is the emissivity coefficient of the particle; $T_{\mathrm{h}}$ and $T_{\mathrm{l}}$ are temperatures of particle and liquid, respectively, (K); $\sigma$ is the radiation heat transfer constant of black body, equal to $5.67\times10^{-8}\ \mathrm{W\cdot K^{-4}\cdot m^{-2}}$; $h_{\mathrm{fg}}$ is the latent heat of vaporization ($\mathrm{J\cdot kg^{-1}}$).

The steady film growth required for a particle entirely penetrating into the coolant is

$$v_{\mathrm{a}} = v_{\mathrm{as}}\left(1 - \alpha_{\mathrm{v}}\right)^{n} \tag{4}$$

where $v_{\mathrm{as}}$ is the value obtained from the single bubble growth model and $n$ is an empirical constant. All results in this paper are based on $n = 0$.

## 3 Experimental

According to the theory of evaporation on the surface of particles, an upward force, which usually disappears in normal conditions, can resist the immersion of the particles. In order to verify the model, we designed a special equipment and performed an observable experiment by pouring one or several high-temperature particles into a water pool. A stove for heating the particles was designed to produce a temperature above 2500 K. The particle's falling down speed was recorded by a high-speed camera.

### 3.1 Test apparatus

The experiments are performed using a particular test apparatus whose conceptual scheme is shown in Fig.1. The facility consists of a test vessel, a furnace and a valve system. The test vessel is a water pool with an inner cross section of 30 cm×30 cm and a height of 100 cm. The water pool is made of a stainless steel frame and 20 cm×70 cm transparent plexiglass panels. Three electric heaters of 3 kW each are equipped at the bottom of the pool to heat up and maintain the water temperature. Ten thermocouples are located up-down symmetrically at the wall surface of the pool to monitor the water temperature. Two pressure transducers are located at the top of the pool to measure the pressure variation. The pressure vessel is designed for 0.2 MPa at 393 K. At the top surface of the vessel, there is a 100 mm-diameter opening connected to a vent pipe, which further connects to the furnace. The vent pipe's height can be adjusted.

The high-temperature furnace (Fig.2) located above the water pool can heat ten 1 mm ~10 mm diameter particles. To protect from the chemical reaction of the particles with the furnace lining and crucible material made of graphite, zirconia is used as the sphere material. The furnace is a cylinder — 680 mm in length and 460 mm in diameter, and consists of two parts, one of which is heating room, inside equipped with graphite heaters and thermal insulators, and the other is release room.

The furnace's heating room consists of a cylindrical graphite heater element, inside of which is a plumbago crucible containing the zirconia spheres. The spheres are heated up in an argon atmosphere.

The 3-phase electric power supply has a maximum power of 12 kW in furnace.

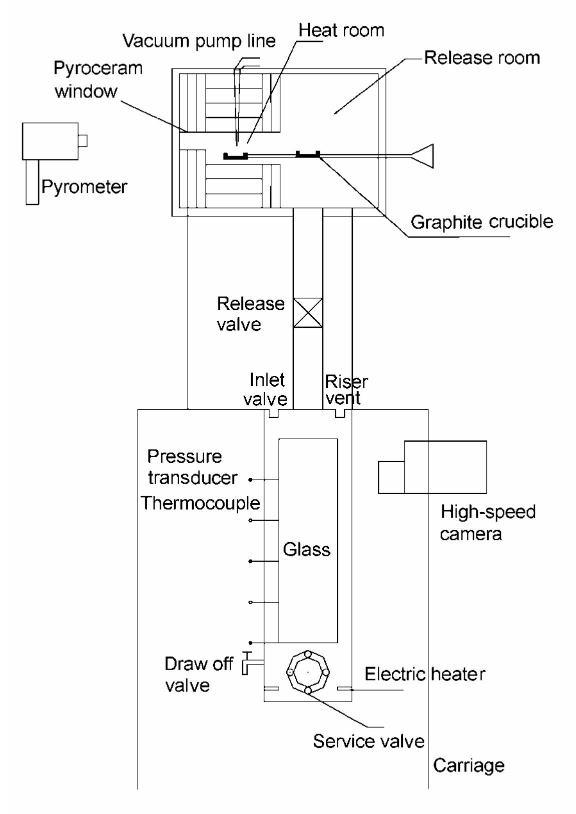


**Fig.1** Scheme of the experiment facility.

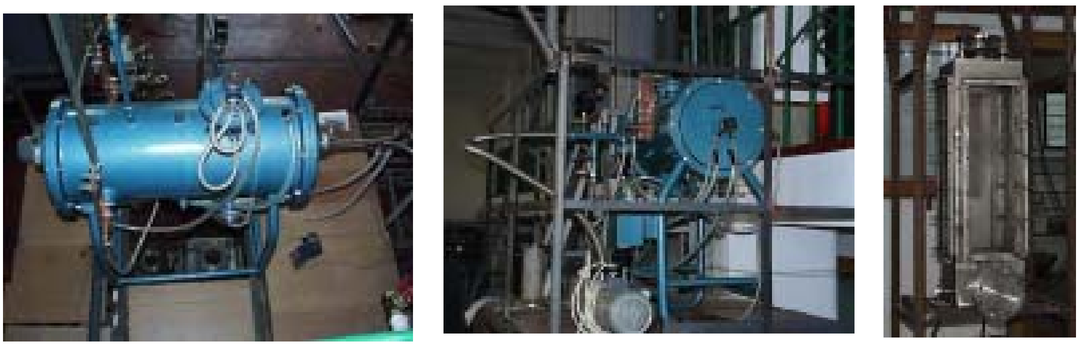

**Fig.2** The experiment facility (a high-temperature furnace and a water pool).

Maximum achievable temperature in the heating room is 2500 K. The sphere temperature is monitored by an optical pyrometer measuring through pyroceram window on the wall of the furnace's heat room. When the spheres are heated up to the predicted temperature, the crucible will be moved to the release room and be released further. The spheres are released while the valve opens. The spheres can drop into the water by gravity.

Behavior of the sphere can be observed from the front side of the water pool using a high-speed camera at 500 /1000 frames per second.

### 3.2 Design of experiments

A total of six experiments with hot spheres, to investigate the premixing phase of a steam explosion, have been performed in the facility. Experiments regarding a number of cold spheres falling into liquid pool have been performed under the same conditions, which are taken as benchmark and to calibrate the measurement systems. Ten experiments were carried out using three types of sphere at different temperatures and different velocities of $\approx$5.61 m·s$^{-1}$, and 6.20 m·s$^{-1}$, respectively. The data on the initial conditions and results of the ten experiments described in this paper are shown in Table 1.

**Table 1** Data of ten experiments

| No. | $\phi$ (mm) | Sphere temperature in furnace (K) | Sphere temperature above water (K) | Water temperature (K) | Sphere velocity above water (m·s$^{-1}$) | Final velocity of penetrating water (m·s$^{-1}$) (Experimental data) | Final velocity of penetrating water (m·s$^{-1}$) (Calculated data) |
|---|---|---|---|---|---|---|---|
| 1 | 10 | 1783 | 1673 | 363 | 5.33 | 4.50 | 4.23 |
| 2 | 10 | 2346 | 2096 | 359 | 5.61 | 4.75 | 4.48 |
| 3 | 10 | 1457 | 1396 | 363 | 6.20 | 5.20 | 4.61 |
| 4 | 10 | 299 | 299 | 363 | 6.20 | 5.40 | — |
| 5 | 5 | 1773 | 1581 | 362 | 5.61 | 4.33 | 4.31 |
| 6 | 5 | 2273 | 2073 | 305 | 5.51 | 4.00 | 4.30 |
| 7 | 5 | 290 | 290 | 363 | 5.51 | 5.50 | — |
| 8 | 5 | 299 | 299 | 363 | 6.20 | 5.62 | — |
| 9 | 3 | 2173 | 1456 | 342 | 5.61 | 3.30 | 3.96 |
| 10 | 3 | 299 | 299 | 363 | 6.20 | 4.75 | — |

## 4 Experimental results

### 4.1 Cold spheres

To better understand the experiments with hot spheres, some results from cold spheres are presented first. Fig.3 shows the typical behavior of a sphere falling into water. The sphere touches the water surface with a velocity of 5.51 m·s$^{-1}$. The final penetrating velocity of the particle was measured to be 5.50 m·s$^{-1}$.

### 4.2 One hot sphere

A $ZrO_2$ sphere was heated up to 2273 K in the furnace, and then was released from 1.55 m up above the water surface. The hot sphere dropped into the 305 K water by gravity. Considering the heat loss by heat convection and radiation heat transfer, temperature of the hot sphere was 2073 K while it touched the water surface. Fig.4 shows that a big bubble appeared at the same time, and velocity of the sphere dropped. The final penetrating velocity of the particle was measured to be 4.0 m·s$^{-1}$.

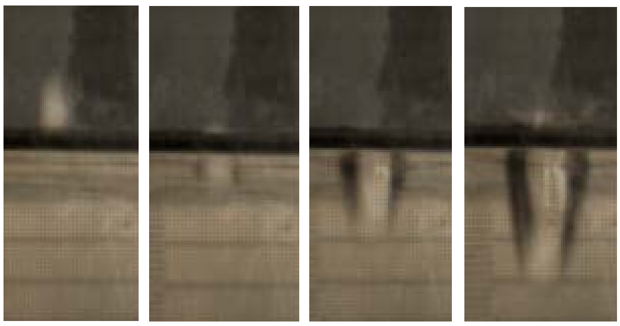

**Fig.3** Four high speed photographs by a high-speed camera with a setting of 1000 frames·s$^{-1}$. A zirconia's sphere is penetrating into water pool, $D_{ZrO_2}$ = 5 mm, $V_{ZrO_{2},0}$ = 5.51 m·s$^{-1}$, $T_{w(water)}$ = 363 K, $T_{ZrO_2}$ = 290 K.

### 4.3 Six hot spheres

Six $ZrO_2$ spheres were heated up to 2273 K in the furnace, then were released from 1.55 m above the water surface. The hot spheres dropped into the 305 K water by gravity at the same time. Fig.5 shows that the bubbles caused by hot spheres overlapped each other.

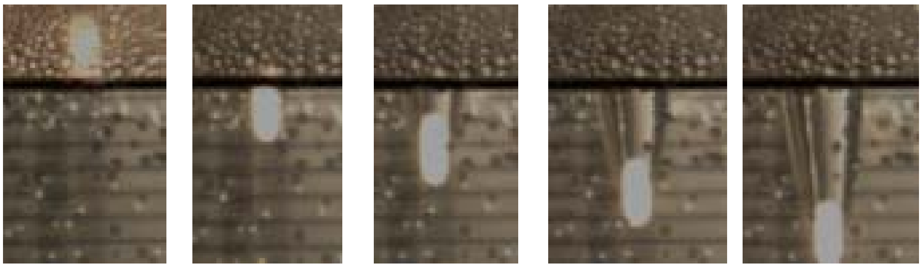

**Fig.4** Five high-speed photographs with 500 frames·s$^{-1}$ camera setting. A zirconia sphere is penetrating into water pool, $D_{ZrO_2}$ = 5 mm, $V_{ZrO_{2},0}$ = 5.51 m·s$^{-1}$ , $T_W$ = 305 K, $T_{ZrO_2}$ = 2073 K.

According to Eq.(2), the final velocity of the particle at the end of the penetration is listed in last column of Table 1. Fig.6 shows the comparison between experimental and calculated data. It was found that the calculated data are close to the experimental ones.

**Fig.5** Steam voids overlap when some high-temperature zirconia's spheres were penetrating into the water pool.

### 4.4 Discussion

The result of the observable experiment manifests that the film thickness profile around the hot sphere is quite different from the cold sphere, because the hot sphere is surrounded by a vapor film with different thickness circumferentially. The experiment and the theoretical analysis show there is a resultant force on the hot sphere, which resists its motion.

Radiation heat transfer plays a very important role in the behavior of very hot particles in contact with water. In Yang's evaporation drag model,[4] radiation heat transfer is taken as the only way to transfer heat from hot particle to the vapor-liquid interface. The calculated results show that the assumption is reasonable for FCI (Fuel and Coolant Interaction) conditions. Fig.6 shows that the experimental and the calculated data are nearly identical. However, the heat conduction and the heat convection must be taken into account when the temperature is dropped.

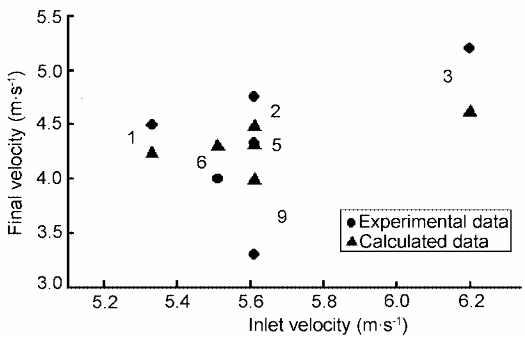


| No. | 1 | 2 | 3 | 5 | 6 | 9 |
|---|---|---|---|---|---|---|
| $D_{ZrO_2}$ (mm) | 10 | 10 | 10 | 5 | 5 | 3 |
| $T_W$ (K) | 363 | 359 | 363 | 362 | 305 | 342 |
| $T_{ZrO_2}$ (K) | 1673 | 2096 | 1396 | 1581 | 2073 | 1456 |

**Fig.6** The final velocity of the high-temperature sphere versus its inlet velocity — a comparison of experimental and calculated data.

In the studies performed by Yang, all of the radiation energy is deposited on the vapor-liquid interface, thus contributing to the vaporization rate and mass balance of the vapor film. In fact, the literature survey by the authors indicates that a significant part of the radiation energy deeply penetrates the body of the liquid. Specifically, for the high-temperature particles with surface temperature about 3000 K, only 25%, 50% and 70% of the radiated energy are deposited within the first millimeter (0.001 m), first centimeter (0.01 m) and first decimeter (0.1 m) of the water behind the vapor-liquid interface, respectively. The vapor film thickness and vapor velocity are determined from the vaporization rate, which is proportional to the energy transferred from the particle leading edge to water by radiation. So, the data of vapor film thickness and vapor velocity calculated by Yang's evaporation drag model[4] are higher than the real data. At the same time, the calculated final penetrating velocity of the particle is lower than the real data.

## 5 Conclusion

In the situations where rapid phase exchanges exist, the drag forces on some components in the system may have many properties different from those shown in general fluid phenomena. The experiments reveal that the drags on a hot sphere, when it contacts with a liquid coolant and the evaporation occurs around the hot sphere, make a large resistance to the motion of the hot sphere, which can not be ignored when the evaporation is extremely rapid (for example, when $T_h$ >1500 K in a water system). Comparisons have been made for the experimental results and the calculations under the evaporation drag model. We found they are nearly identical. The result of experiments encourages us to further investigate and find the particle behavior under the different initial conditions during the evolution of hot-particle /coolant interfacial surface associated heat transfer. The result of pilot study verified the theory of evaporation drag model.

## References

1 Corradini M L, Kim B J. Nucl Saf, 1991, **32**(3): 337-362

2 Severe accident risk: An assessment for five U.S. nuclear power plants, Final Summary Report, NUREG-1150. Vol.1, U.S. NRC, 1990,12

3 Meyer L. The Interaction of a Falling Mass of Hot Spheres with Water. Proc Natl Heat Transfer Conf, American Nuclear Society, Houston, Texas, USA, 1996, **9**: 105-134

4 Yang Y H. Multi-phase simulations for phenomena in vapor explosions, University of Tokyo, Doctoral Dissertation, 1996